Icarus 211 (2011) 798–803

Contents lists available at ScienceDirect

Icarus

journal homepage: www.elsevier.com/locate/icarus

The phase diagram of water and the magnetic fields of Uranus and Neptune

Ronald Redmer [a,*], Thomas R. Mattsson [b], Nadine Nettelmann [a,c], Martin French [a]

[a] Universität Rostock, Institut für Physik, D-18051 Rostock, Germany
[b] Pulsed Power Sciences Center, Sandia National Laboratories, Albuquerque, NM 87185-1189, USA
[c] Department of Astronomy and Astrophysics, University of California, Santa Cruz, CA 95064, USA

ARTICLE INFO

Article history:
Received 12 January 2010
Revised 18 August 2010
Accepted 18 August 2010
Available online 22 August 2010

Keywords:
Neptune, Interior
Uranus, Interior
Magnetic fields

ABSTRACT

The interior of giant planets can give valuable information on formation and evolution processes of planetary systems. However, the interior and evolution of Uranus and Neptune is still largely unknown. In this paper, we compare water-rich three-layer structure models of these planets with predictions of shell structures derived from magnetic field models. Uranus and Neptune have unusual non-dipolar magnetic fields contrary to that of the Earth. Extensive three-dimensional simulations of Stanley and Bloxham (Stanley, S., Bloxham, J. [2004]. Nature 428, 151–153) have indicated that such a magnetic field is generated in a rather thin shell of at most 0.3 planetary radii located below the H/He rich outer envelope and a conducting core that is fluid but stably stratified. Interior models rely on equation of state data for the planetary materials which have usually considerable uncertainties in the high-pressure domain. We present interior models for Uranus and Neptune that are based on *ab initio* equation of state data for hydrogen, helium, and water as the representative of all heavier elements or ices. Based on a detailed high-pressure phase diagram of water we can specify the region where superionic water should occur in the inner envelope. This superionic region correlates well with the location of the stably-stratified region as found in the dynamo models. Hence we suggest a significant impact of the phase diagram of water on the generation of the magnetic fields in Uranus and Neptune.

1. Introduction

All four giant planets in our Solar System have active dynamos. While Jupiter and Saturn exhibit an axial dipolar magnetic field similar to that of the Earth, Voyager 2 revealed a non-dipolar and non-axisymmetric magnetic field structure of Uranus and Neptune. Since magnetic fields are generated by the motion of conducting fluids inside the planet, substantial differences in their interior structure and composition must exist. Understanding the complex planetary dynamo processes in Uranus and Neptune would give us additional constraints for interior models which in turn are based on assumptions about their composition and on equation of state (EOS) data for the planetary materials.

The construction of acceptable interior models is a great challenge (Stevenson, 1982; Gudkova and Zharkov, 1999; Guillot, 1999a; Guillot, 1999b). They rely on our knowledge of observational parameters that are sufficiently known for the four outer planets in the Solar System in order to depict certain ranges of mass distributions. Those mass distributions allow the internal bulk composition to be inferred. As a result, we distinguish between gas giants like Jupiter and Saturn which are mainly composed of hydrogen and helium, and ice giants like Uranus and Neptune which contain more heavy elements in form of rock and the ices H_2O and CH_4, or iron-rock planets such as the Earth.

The most important input into interior models are the thermal and caloric EOS $P(\varrho, T)$ and $U(\varrho, T)$, respectively, for the relevant materials. Progress in shock-wave experimental technique has allowed the region up to several megabars to be probed, especially the most abundant cosmological elements and molecules H, He, and H_2O which are also the most abundant elements and compounds in giant planets (Fortov et al., 2003; Nellis, 2006). Laboratory studies for materials at conditions deep in planetary interiors, i.e. exceeding 10 Mbar, are planned at facilities such as the Z machine (Bailey et al., 2009) and the National Ignition Facility (Moses et al., 2009) based on novel X-ray scattering experiments (Fortney et al., 2009; Glenzer and Redmer, 2009). Furthermore, *ab initio* simulations can now be performed almost routinely to determine high-pressure EOS data (Oganov et al., 2005; Gillan et al., 2006; Nettelmann et al., 2008).

Uranus and Neptune are of special interest in this context. Neptune serves as a prototypical ice giant planet as indicated by its strong atmospheric carbon enrichment of about 25 times solar (Podolak and Reynolds, 1981). Extrasolar giant planets similar in mass and radius such as GJ 436b or HAT-P-11b have been observed recently. Uranus bears unique information on planet formation and

* Corresponding author. Fax: +49 381 4986912.
E-mail addresses: ronald.redmer@uni-rostock.de (R. Redmer), trmatts@sandia.gov (T.R. Mattsson), nadinen@ucolick.org (N. Nettelmann), martin.french@uni-rostock.de (M. French).

0019-1035/$ - see front matter © 2010 Elsevier Inc. All rights reserved.
doi:10.1016/j.icarus.2010.08.008

evolution in a sense that conventional scenarios fail to explain its low intrinsic luminosity (Hubbard et al., 1995). Recent interior models based on *ab initio* EOS data (Fortney and Nettelmann, 2010) indicate a very strong heavy element enrichment in the deep interior. However, mass distributions remain ambiguous with respect to composition, e.g. a mixture of silicates and H/He can yield the same pressure–density relation as that of water, and further constraints are absolutely essential.

Such conditions can be derived for the interior of Uranus and Neptune from its non-dipolar and non-axisymmetric magnetic field. Hubbard et al. (1995) proposed that the heat flow data from both ice giants indicate an interior that is only partially convective. Based on that assumption Stanley and Bloxham (2004), Stanley and Bloxham (2006) performed three-dimensional simulations of Neptune's and Uranus' dynamo in thin-shell geometries surrounding a stably stratified inner region. They found that dynamos in such a geometry could produce non-dipolar, non-axisymmetric magnetic fields as typical for both ice giants, in cases where the stable layer is fluid, of similar conductivity as the dynamo generating region, and extends to about 0.4–0.55 of the planet radius. Based on these fundamental results, further interesting problems have to be studied. We here investigate whether or not the results are also consistent with transport properties of the materials assumed for planet interior and evolution models. For the bulk composition, conventional Uranus and Neptune models (Hubbard and MacFarlane, 1980; Hubbard et al., 1995) assume H/He-rich atmospheres, an ice-rich deep interior, and a central rock core, where ices are mixtures of H_2O, CH_4, and NH_3 or pure water. In conventional interior and evolution models, equations of state for these materials are perturbed polytropic zero-temperature relations that reproduce available shock compression data of single materials (Hubbard and MacFarlane, 1980) or mixtures (Hubbard et al., 1995) fairly well. The thermal contribution to the pressure is obtained by the choice of appropriate values for the Grueneisen parameter γ and the specific heat capacity c_V of molten ice which again can be estimated from shock data (Hubbard and MacFarlane, 1980). We here present, for the first time, the electric conductivity of warm dense water derived from *ab initio* simulations and compare the planetary shell structure according to the phase diagram of water with the predictions from the dynamo models.

2. Interior model

We have modeled the interior of a planet of mass M_P and equatorial radius $R_{\rm eq}$ assuming the standard three-layer structure (Stevenson, 1982; Guillot, 1999a,b; Nettelmann et al., 2008), i.e. a rocky core surrounded by two fluid envelopes. We have solved the hydrostatic equation for a rotating planet,

$$\frac{1}{\varrho(\mathbf{r})}\nabla P(r) = -\nabla(V(\mathbf{r}) + Q(\mathbf{r})), \tag{1}$$

$$V(\mathbf{r}) = -G\int_V d^3r' \frac{\varrho(\mathbf{r}')}{|\mathbf{r}-\mathbf{r}'|}, \quad Q(\mathbf{r}) = -\frac{1}{2}\omega_{pl}^2 r^2 \sin^2(\theta), \tag{2}$$

where $V(\mathbf{r})$ and $Q(\mathbf{r})$ are the gravitational and centrifugal potentials, $P(\mathbf{r})$ is the pressure at the radius $\mathbf{r}$, and $\varrho(\mathbf{r}) = m(\mathbf{r})/V$ is the mass density in the mass shell $m(\mathbf{r})$. The planet rotates with an angular velocity ω_{pl}, and θ is the angle with the rotation axis. We have expanded the gravitational field imposed by the density distribution $\varrho(\mathbf{r})$ by means of Legendre polynomials $P_n(x)$ as usual so that it can be expressed by gravitational moments J_n,

$$V(r,\theta) = -\frac{Gm(r)}{r^2}\left(1 - \sum_{n=1}^{\infty}\left(\frac{R_{\rm eq}}{r}\right)^{2n} J_{2n}P_{2n}(\cos\theta)\right), \tag{3}$$

$$J_n = -\frac{1}{MR_{\rm eq}^n}\int_V d^3r' \varrho(r')(r')^n P_n(\cos\theta'). \tag{4}$$

The gravitational potential (4) was calculated on equipotential (level) surfaces $l(r,\theta)$ by using the theory of figures (Zharkov and Trubitsyn, 1978),

$$r_l(\theta) = l\left(1 + \sum_{n=0}^{\infty} s_{2n}(l)P_{2n}(\cos\theta)\right). \tag{5}$$

The expansion coefficients are the figure functions $s_n(l)$ which were determined up to third order, i.e. $n = 3$. An iterative procedure ensures convergence of the figure functions of better than 0.1% for s_2 and s_4, and 1% for s_6.

The interior models for Neptune (Uranus) were constructed assuming the following three-layer structure which closely resembles the models by Hubbard et al. (1995): An outer adiabatic H/He envelope with a water mass fraction of 0.4 (0.10), an inner adiabatic H/He envelope with a water mass fraction of 0.9 (0.876), and an isothermal rocky core of mass 1.28 $M_\oplus$ (1.94 $M_\oplus$). The model values of the constraining parameters planet mass M_p, mean radius R_p, 1-bar temperature T_1, angular velocity ω_{pl}, and gravitational moments J_2 and J_4 are within the observational uncertainties (see e.g. Guillot and Gautier, 2007). The He/H mass ratio is assumed to be 0.275 throughout the envelopes in agreement with atmospheric He abundance measurements and the protosolar cloud value (Gautier et al., 1995).

Apart from the random density distribution models by Podolak et al. (2000), Uranus and Neptune structure and evolution models have been constructed exclusively on the simplified assumption of adiabatic, homogeneous envelopes. This assumption has been found to give cooling times of these planets beyond the age of the Solar System if the planets are ice-rich and started off at high internal temperatures as expected from the mass accretion processes during formation. In turn, the cooling time of Uranus and Neptune can sufficiently shorten if the ice to rock ratio is highly subsolar (Hubbard and MacFarlane, 1980), or the planets started at low internal temperatures (Hubbard and MacFarlane, 1980; Hubbard et al., 1995), or the inner $\sim$ 60% (Uranus) or 50% (Neptune) of the planet's radius is prevented from cooling (Hubbard et al., 1995). While the first two possibilities are disfavoured by planet formation theory (Podolak et al., 1991), the latter possibility contradicts the assumption of a fully adiabatic, homogeneous deep envelope. Nevertheless, we adopt the standard approach in this paper and discuss its implications in Section 4.

3. Ab initio equation of state data

To construct interior models, EOS data are required for all relevant materials in the planet, i.e. for H, He, and water as in the case of Uranus and Neptune, and for a wide range of pressures and temperatures: From nearly normal conditions in the surface region (70 K and 1 bar) up to extreme parameters of (5–6) $\times$ 10^3 K and 5–7 Mbar as found in the cores. Besides the Sesame tables (Lyon and Johnson, 1992) which provide approximate wide-range EOS data and advanced chemical models (Saumon et al., 1995; Holst et al., 2007) that yield EOS data based on effective pair potentials, *ab initio* methods were successfully applied to calculate thermophysical properties of matter under such extreme conditions. Especially, the high-pressure EOS data for hydrogen (Holst et al., 2008), helium (Kietzmann et al., 2007), hydrogen–helium mixtures (Lorenzen et al., 2009), and water (French et al., 2009) as the representative of ices were derived from extensive finite-temperature density functional theory molecular dynamics (FT-DFT-MD) simulations for which we have used the Vienna Ab initio Simulation Package (VASP) (Kresse and Hafner, 1993; Kresse and Furthmüller, 1996; Hafner, 2008). This *ab initio* EOS data were used recently to construct an interior model for Jupiter (Nettelmann et al., 2008) and the extrasolar planet GJ 436b (Nettelmann et al., 2010).

The FT-DFT-MD method combines classical MD simulation for the ions and a quantum treatment for the electrons based on FT-DFT. The electron density

$$\varrho_{\rm el}(\mathbf{r}) = \sum_{i,\mathbf{k}} |\Psi_{i,\mathbf{k}}(\mathbf{r})|^2 f_{i,\mathbf{k}} \tag{6}$$

is given by the Kohn–Sham orbitals $\Psi_{i,\mathbf{k}}(\mathbf{r})$ weighted with the Fermi distribution function $f_{i,\mathbf{k}} = [\exp(E_{i,\mathbf{k}} - \mu)/k_B T + 1]^{-1}$; i is the band index. The effective one-particle orbitals are determined by solving the respective Kohn–Sham equations (Kohn and Sham, 1965) for each MD step and the corresponding ion distribution in the simulation box, i.e. the ions are located at positions $\mathbf{R}_I$:

$$\begin{aligned} &\left[-\frac{\hbar^2}{2m}\nabla^2 + V_{\rm eff}(\mathbf{r})\right]\Psi_{i,\mathbf{k}}(\mathbf{r}) = E_{i,\mathbf{k}}\Psi_{i,\mathbf{k}}(\mathbf{r}), \\ &V_{\rm eff}[\varrho_{\rm el}(\mathbf{r})] = \int d^3r' \frac{\varrho_{\rm el}(\mathbf{r}')e^2}{|\mathbf{r}-\mathbf{r}'|} - \sum_{I=1}^{N}\frac{Z_I e^2}{|\mathbf{r}-\mathbf{R}_I|} + V_{XC}[\varrho_{\rm el}(\mathbf{r})], \end{aligned} \tag{7}$$

where e is the electron charge and m its mass. The first term in the effective interaction potential denotes the classical electron–electron interaction, the second one is the electron–ion interaction, and the third term, the exchange-correlation potential $V_{XC}[\varrho_{\rm el}(\mathbf{r})]$, represents all quantum and higher-order correlation effects. We have used the generalized gradient approximation exchange-correlation functional in the parameterization of Perdew et al. (1996) in the DFT calculations.

When an electronic structure calculation is fully converged, ions are moved according to the forces acting on them which are determined via the Hellmann–Feynman theorem. Repeating this procedure for several thousand timesteps of about 1 fs yields typical simulation times of up to 10 ps. After the simulations reach thermodynamic equilibrium, thermodynamic quantities such as pressure and internal energy are derived from mean values averaged over the following several thousand timesteps. Up to 512 electrons can routinely be considered in the cubic simulation box with periodic boundary conditions; we have used up to 54 molecules for the calculation of the water EOS (Nettelmann et al., 2008; French et al., 2009).

Convergence of the FT-DFT-MD method is an important issue and was verified with respect to the **k**-point sets used for the evaluation of the Brillouin zone and the energy cutoff for the plane wave basis set. For the determination of the EOS data we have chosen the Baldereschi mean value point (Baldereschi, 1973) for H and He, the Γ point for water, energy cutoffs of 700 eV (He), 900 eV (H_2O), and 1200 eV (H), as well as the standard pseudopotentials supplied with VASP. We estimate that the convergence of the EOS data is better than 5% (Nettelmann et al., 2008).

The electrical conductivity is an important input into dynamo models. If dissociation of molecules occurs in the interior of water-rich planets, we have to consider both the electronic and ionic contribution. The frequency dependent electronic conductivity $\sigma_{\rm el}(\omega)$ was derived from an evaluation of the Kubo–Greenwood formula (Kubo, 1957; Greenwood, 1958) for the relevant pressure and temperature domain,

$$\begin{aligned} \sigma_{\rm el}(\omega) = \frac{2\pi e^2\hbar^2}{3m^2\omega\Omega}\sum_{\mathbf{k}} W(\mathbf{k}) \sum_{j=1}^{N}\sum_{i=1}^{N}\sum_{\alpha=1}^{3}[f_{i,\mathbf{k}} - f_{j,\mathbf{k}}] \\ \times |\langle\Psi_{j,\mathbf{k}}|\nabla_\alpha|\Psi_{i,\mathbf{k}}\rangle|^2 \delta(E_{j,\mathbf{k}} - E_{i,\mathbf{k}} - \hbar\omega). \end{aligned} \tag{8}$$

The summations over i and j run over N discrete bands considered in the electronic structure calculation for the cubic supercell of volume Ω. The three spatial directions are averaged by the α sum. The Fermi distribution function $f_{i,\mathbf{k}}$ describes the occupation of the ith band corresponding to the energy $E_{i,\mathbf{k}}$ and the wavefunction $\Psi_{i,\mathbf{k}}$ at **k**. The δ-function has to be broadened because a discrete energy spectrum results from the finite simulation volume. Integration over the Brillouin zone was performed by sampling special **k** points (Monkhorst and Pack, 1976), where $W(\mathbf{k})$ is the respective weighting factor. Again, we have used Baldereschi's mean value point (Baldereschi, 1973) to reach a convergence of better than 10% accuracy for the electronic conductivity; for details, see Desjarlais et al. (2002), Holst et al. (2008), Lorenzen et al. (2009), and French et al. (2010).

The ionic (protonic) conductivity is of major importance in water at conditions deep in planetary interiors. It was determined applying the method of Mattsson and Desjarlais (2006) for the calculation of the ionic diffusion coefficients and assuming a generalized Einstein relation; see French et al. (2010) for details.

Considering the interiors of Uranus and Neptune, the high-pressure EOS and the electrical conductivity of water are of particular importance. Since the first prediction of an exotic superionic phase at several Mbar (Cavazzoni et al., 1999), the behavior of water under extreme conditions has attracted much attention (Goldman et al., 2005; Mattsson and Desjarlais, 2006; French et al., 2009, 2010). We show the pressure–temperature phase diagram of water as derived from extensive FT-DFT-MD simulations in Fig. 1. High-pressure ice phases occur only below 2500 K. Above 3000 K, our results indicate that water is either strongly dissociated (fluid or plasma) or in the superionic state. Dissociation of water molecules can be inferred from the systematic difference between the diffusion coefficients of both ion species. The superionic water phase is characterized by an oxygen lattice through which the protons diffuse almost freely. Therefore, superionic water can be considered as a two-component system of both a conducting proton fluid and a crystalline oxygen solid.

The combination of a proton fluid and an oxygen lattice in the superionic phase raises the question of the character of this hybrid phase, especially with respect to its response to electromagnetic stress. We therefore performed first-principles calculations of the shear viscosity in the same manner as Alfé and Gillan (1998). For conditions along the isentrope, we find viscosity values of about 2 mPa s for warm dense fluid water (at 3000 K and 2.5 g/cm^3) and of about 1 mPa s within the superionic phase (at 4000 K and 3.5 g/cm^3). We conclude that the superionic phase responds almost like a fluid.

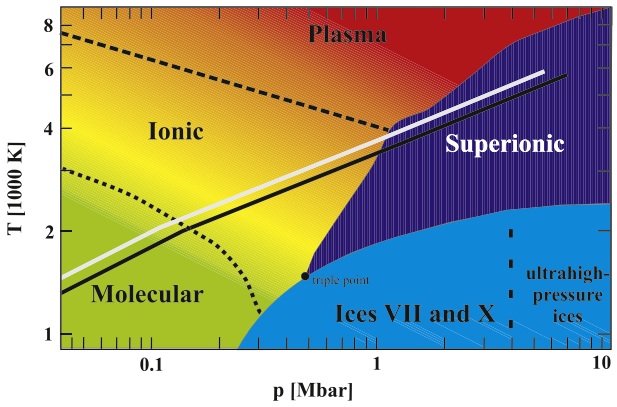

Fig. 1. Phase diagram of water up to high pressures as relevant for the interiors of Uranus and Neptune. The solid (ice VII and X), fluid (molecular, ionic, plasma), and superionic phase are shown by different colors. The dotted line indicates the continuous transition due to dissociation (more than 20% of the water molecules dissociated), the broken line that due to ionization (electronic conductivity >100/Ωcm) in the dense fluid. The calculated isentrope for Neptune (Uranus) is shown by a thick black (gray) line. The location of the triple point between ice, fluid, and superionic water is not well determined yet (Schwager et al., 2004; Goncharov et al., 2005; Lin et al., 2005; Schwegler et al., 2008; Schwager and Boehler, 2008; Goncharov et al., 2009). The predicted ice structures at ultrahigh-pressures beyond 4 Mbar (Benoit et al., 1996) and possible triple points with superionic water are not well known so far and subject of future work.

Due to the limited particle numbers in the FT-DFT-MD simulations, we can determine the boundaries between the various water phases only within an estimated uncertainty of 10–20%. Jumps in the internal energy indicate that the transition between the ionic fluid or plasma and the superionic water is of first order.

The corresponding isentropes through Neptune and Uranus are shown in Fig. 1. They have two remarkable features: the adiabatic gradients rise such that no boundaries to ice phases (e.g. ice VII or X) are crossed, and they both run into the superionic phase. We will discuss the impact of these results in the next section.

4. Interior structure and planetary magnetic field

4.1. Results

Fig. 2 shows possible compositions of Uranus and Neptune along the linearly running radius coordinate. A full arc corresponds to 100% in mass for a given radius level. Numbers on the left are radius in planetary radii R_U and R_N, respectively; numbers on the right are temperatures in K and pressures in Mbar at the surface and at both layer boundaries as defined by the change in composition. Our results for the phase diagram of water and the calculated $P-T$ profile displayed in Fig. 1 imply a further discrimination within the inner envelope. This layer consists of two shells: The upper one contains molecular water which transforms continuously into an ionic fluid (yellow), while the lower one is composed of superionic water (indigo). The transition to superionic water occurs slightly above half the radius: for this particular Neptune model at about $0.62R_N$ and 1.4 Mbar and 3760 K, and for Uranus at about $0.57R_U$ and 1.45 Mbar and 4000 K. These parameters determine the shell boundaries. Within the range of possible Uranus and Neptune models found (Fortney and Nettelmann, 2010), the shell boundaries change by no more than a few percent. The smaller left slices show the shell boundaries of models 5 (Uranus) and 6 (Neptune) investigated by Stanley and Bloxham (2006), cf. their Table 3, assuming that they are among the very few ones that reproduce the magnetic field structure.

We find a remarkable agreement of our interior models based on *ab initio* EOS data with the thin-shell geometries that were assumed by Stanley and Bloxham (2004), Stanley and Bloxham (2006) in their dynamo models: (i) a small – or even absent – solid core in the center; (ii) a fluid shell which extends from about 0.42–0.56 to 0.7–0.8 of the planet radius (here: the ionic water shell extending from $\sim$0.6 to $0.8R_p$), in which the conductivity is sufficiently (at least 20 $(\Omega\text{cm})^{-1}$) high for sustaining a dynamo process, and (iii) a fluid region of similar conductivity as the surrounding dynamo generating shell extending to less than $0.8\times(0.7\text{–}0.8)R_p$ (here: the superionic shell with its mobile proton fluid extending up to $\sim 0.57R_p$ in Uranus and $\sim 0.62R_p$ in Neptune).

The apparent correlations between the dynamo models and the interior models have motivated us to calculate the electrical conductivity for pressure–temperature conditions along the planetary adiabats, see Fig. 3. Both the electronic (via Eq. (8)) and ionic contributions (via a generalized Einstein relation) were taken into account. While the outer molecular envelope is insulating, the convecting shell of the inner envelope beneath is mainly composed of dissociated water with a typical ionic conductivity of about (10–120)/Ωcm. The superionic shell has a slightly higher, mostly protonic conductivity of (120–350)/Ωcm and can thus well respond to magnetic stress. Taking into account that the conductivity of H/He or, on the other hand, rock-dominated planetary material at Mbar pressures in that layer might be different by several orders of magnitude, we consider already the present correlation a serious indication of the importance of understanding water under extreme conditions for the interior structure and magnetic field generation in Neptune-like planets. Thus, we have given a possible physical explanation for the finding of Stanley and Bloxham (2004, 2006) that the thin convecting fluid layer and the extended stably stratified layer beneath have similar conductivities.

4.2. Discussion

Stanley and Bloxham (2006) furthermore require stability against convection of the deep shell as this was suggested by homogeneous evolution calculations by Hubbard et al. (1995). Of course, the responsibility for stable stratification can lie in processes that are unrelated to the superionic phase. For instance, despite its oxygen lattice structure, pure superionic water heated from below by the inner core is not necessarily stable to convection as was demonstrated for the similar crystalline structures of ice X and ice VII (Fu et al., 2010). Stable stratification implies sub- or superadiabaticity depending on the process causing stability. If for instance, convection is suppressed by a compositional gradient (inhomogeneity), heat within or below the stable region is largely prevented from efficient outward transport and hence the temperature gradient will be super-adiabatic. Is the superionic shell consistent with inhomogeneity? In superionic water mixed with H/He and other ices, immiscibility of materials and subsequent sedimentation can occur invoking a compositional gradient. According to the recent theoretical phase diagram of H–He mixtures (Lorenzen et al., 2009), He would separate from H at deep envelope conditions, while test calculations for H_3O and H_4O have indicated that the occurrence of a superionic phase is robust against hydrogen enrichment. A determination of the miscibility and sedimentation

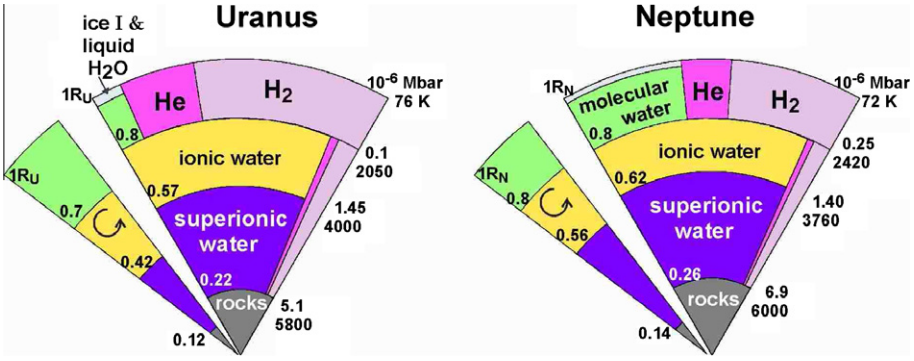

Fig. 2. Composition throughout Uranus and Neptune. Broad slices illustrate standard three-layer models based on our *ab initio* EOS data that reproduce the gravity field data; thin slices on the left illustrate fluid, conducting core model nos. 5 (left) and 6 (right) proposed by Stanley and Bloxham (2006). The radius coordinate of models 5 and 6 is scaled such that the outer boundary of the magnetic field generating thin shells corresponds to $0.7R_U$ for Uranus and $0.8R_N$ for Neptune, see Stanley and Bloxham, 2006. The color code highlights shells of similar properties with respect to convective instability, conductivity, and composition.

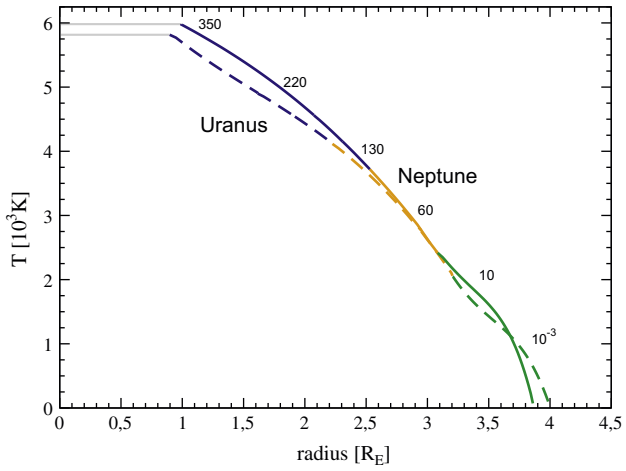

Fig. 3. Electrical conductivity along the isentropes of Uranus and Neptune. Numbers are given in units of 1/Ωcm; they apply to both planets in good approximation. The value 10^{-3} for molecular water was taken from reference Holzapfel (1969). The color code refers to the water phase diagram shown in Fig. 1: outer shell of insulating molecular water (green), ionic water shell beneath (yellow), and superionic water shell (blue). The isothermal core regions are indicated by gray lines.

behavior of relevant materials in the interior would require substantial additional efforts which go far beyond the scope of the present study. We conclude stable stratification due to inhomogeneity by sedimentation can occur in – while not necessarily caused by – a deep superionic shell.

If on the other hand, the medium remains convectively stable because of a shallow temperature gradient, internal present temperatures will be lower than in the adiabatic case. Subadiabaticity implies efficient heat transport by radiation or conduction. Guillot et al. (1994) found radiative windows in Uranus and Neptune around 1500 K, which close toward lower temperatures because of strong infrared absorption by ice molecules, and toward higher temperatures because of rising free electron abundances enhancing collision induced absorption. Hence according to former calculations, a subadiabatic temperature profile inhibiting convection might occur in the outer, molecular envelope, but not in the deep interior. In the superionic phase however, the electrons are located preferentially close to the oxygen ions – they *glue* the oxygen lattice (Mattsson and Desjarlais, 2006; French et al., 2010). Compared to normal ionic water, the electronic conductivity is decreased and the transparency to photon transport increased. Furthermore, our test calculations for the viscosity suggest that the superionic phase is fluid enough to respond to changes in the electromagnetic stress through *fluid* motion to avoid anchoring the magnetic field to the core. Future studies will show if superionic water with some admixture of H and He is sufficiently transparent to cause stable stratification and whether or not its almost fluid-like structure (viscosity) corresponds with the assumptions made for the deep shell in the dynamo models.

As described in Section 2, homogeneous evolution of fully adiabatic interiors leads to long cooling times of Uranus and Neptune, and even lower internal temperatures will prolong the time needed to cool down from an initially hot interior down to the present state even more. Hence if stable stratification in the deep interior occurs because of a radiative superionic shell extending up to $\sim 0.6 R_p$, further improvements of Uranus and Neptune interior models are necessary in order to achieve consistency with the current heat flux of the planets. Recent homogeneous evolution calculations (Fortney and Nettelmann, 2010) of Uranus and Neptune based on the same EOS data as used in this work confirm previous results for Uranus, while for Neptune the cooling time has improved to about 5.5 Gyr. Those structure models (as well as the ones presented here) have an ice to rock ratio of two times solar. Thus the direction proposed by Hubbard and MacFarlane (1980) of lowering the specific heat capacity of the interior by lowering the ice to rock ratio can potentially bring the cooling time in agreement with the age of the Solar System even in case of a superionic radiative layer, in particular for Neptune. Quantitative results will be our future work. We furthermore encourage magnetic field modelers to search for further geometries that reproduce the magnetic field of Uranus and Neptune, in particular to (re-)investigate the effect of the conductivity and the extension of the deep interior.

5. Conclusions

In conclusion, we have shown that additional constraints derived from Uranus' and Neptune's unusual magnetic field are in agreement with a three-layer interior model based on *ab initio* EOS data for hydrogen, helium, and water. An extended superionic water layer is likely to occur deep in the interior of Neptune-like planets. The results for the electrical conductivity along Uranus' and Neptune's isentrope comply with the results of the magnetic field simulations. The present results show that advanced interior models can be constructed if – besides the usual observational constraints such as the gravity data – also details of the planetary magnetic field structure are taken into account. Such kind of advanced models would include non-adiabatic deep shells with heat and radiation transport according to the thermophysical transport properties of water under high pressure. Evolution calculations will also help to validate advanced interior models.

Acknowledgments

We thank W. Lorenzen, B. Holst, R. Neuhäuser, M.P. Desjarlais and V.E. Fortov for helpful discussions and comments. This work was supported by the Deutsche Forschungsgemeinschaft (DFG), the Supercomputing Center North (HLRN), and the Computing Center of the University of Rostock. This work was supported by the NNSA Science Campaigns. Sandia National Laboratories is a multi-program laboratory operated by Sandia Corporation, a wholly owned subsidiary of Lockheed Martin company, for the US Department of Energy's National Nuclear Security Administration under Contract DE-AC04-94AL85000.

References

Alfé, D., Gillan, M.J., 1998. First-principles calculation of transport coefficients. Phys. Rev. Lett. 81, 5161–5164.
Bailey, J.E., Rochau, G.A., Mancini, R.C., Iglesias, C.A., MacFarlane, J.J., Golovkin, I.E., Blancard, C., Cosse, P., Faussurier, G., 2009. Experimental investigation of opacity models for stellar interior, inertial fusion, and high energy density plasmas. Phys. Plasmas 16, 058101.
Baldereschi, A., 1973. Mean-value point in the Brillouin zone. Phys. Rev. B 7, 5212–5215.
Benoit, M., Bernasconi, M., Focher, P., Parrinello, M., 1996. New high-pressure phase of ice. Phys. Rev. Lett. 76, 2934–2936.
Cavazzoni, C., Chiarotti, G.L., Scandolo, S., Tosatti, E., Bernasconi, M., Parrinello, M., 1999. Superionic and metallic states of water and ammonia at giant planet conditions. Science 283, 44–46.
Desjarlais, M.P., Kress, J.D., Collins, L.A., 2002. Electrical conductivity for warm, dense aluminum plasmas and liquids. Phys. Rev. E 66, 025401.
Fortney, J.J., Nettelmann, N., 2010. The interior structure, composition, and evolution of giant planets. Space Sci. Rev. 152, 423–447.
Fortney, J.J., Glenzer, S.H., Koenig, M., Militzer, B., Saumon, D., Valencia, D., 2009. Frontiers of the physics of dense plasmas and planetary interiors: Experiments, theory, and applications. Phys. Plasmas 16, 041003.
Fortov, V.E., Ternovoi, V.Y., Zhernokletov, M.V., Mochalov, M.A., Mikhailov, A.L., Filimonov, A.S., Pyalling, A.A., Mintsev, V.B., Gryaznov, V.K., Iosilevskii, I.L., 2003. Pressure induced ionization of nonideal plasma in a megabar range of dynamic pressures. J. Exp. Theor. Phys. 97, 259–278.

French, M., Mattsson, T.R., Nettelmann, N., Redmer, R., 2009. Equation of state and phase diagram of water at ultrahigh pressures as in planetary interiors. Phys. Rev. B 79, 054107.
French, M., Mattsson, T.R., Redmer, R., 2010. Diffusion and electrical conductivity in water at ultra-high pressures. Phys. Rev. B, submitted for publication.
Fu, R., O'Connell, R.J., Sasselov, D.D., 2010. The interior dynamics of water planets. Astrophys. J. 708, 1326–1334.
Gautier, D., Conrath, B.J., Owen, T., de Pater, I., Atreya, 1995. The troposphere of Neptune. In: Cruishank, D.P. (Ed.), Neptune and Triton. University of Arizona, Tucson, pp. 547–611.
Gillan, M.J., Alfè, D., Brodholt, J., Vočadlo, L., Price, G.D., 2006. First-principles modelling of Earth and planetary materials at high pressures and temperatures. Rep. Prog. Phys. 69, 2365–2441.
Glenzer, S.H., Redmer, R., 2009. X-ray Thomson scattering in high-energy density plasmas. Rev. Mod. Phys. 81, 1625–1663.
Goldman, N., Fried, L.E., Kuo, I.-F.W., Mundy, C.J., 2005. Bonding in the superionic phase of water. Phys. Rev. Lett. 94, 217801.
Goncharov, A.F., Goldman, N., Fried, L.E., Crowhurst, J.C., Kuo, I.-F.W., Mundy, C.J., Zaug, J.M., 2005. Dynamic ionization of water under extreme conditions. Phys. Rev. Lett. 94, 125508.
Goncharov, A.F., Sanloup, C., Goldman, N., Crowhurst, J.C., Bastea, S., Howard, W.M., Fried, L.E., Guignot, N., Mezouar, M., Yue, M., 2009. Dissociative melting of ice VII under pressure. J. Chem. Phys. 130, 124514.
Greenwood, D.A., 1958. The Boltzmann equation in the theory of electrical conduction in metals. Proc. Phys. Soc. Lond. 71, 585–596.
Gudkova, T.V., Zharkov, V.N., 1999. Models of Jupiter and Saturn after the Galileo mission. Planet. Space Sci. 47, 1201–1210.
Guillot, T., 1999a. A comparison of the interiors of Jupiter and Saturn. Planet. Space Sci. 47, 1183–1200.
Guillot, T., 1999b. Interiors of giant planets inside and outside the Solar System. Science 286, 72–77.
Guillot, T., Gautier, D., 2007. Giant Planets. In: Schubert, G., Spohn, T. (Eds.), Treatise of Geophysics, vol. 10, Planets and Moons, pp. 439–464.
Guillot, T., Gautier, D., Chabrier, G., Mosser, B., 1994. Are the giant planets fully convective? Icarus 112, 337–353.
Hafner, J., 2008. Ab-initio simulations of materials using VASP: Density-functional theory and beyond. J. Comput. Chem. 29, 2044–2078.
Holst, B., Nettelmann, N., Redmer, R., 2007. Equation of state for dense hydrogen and plasma phase transition. Contrib. Plasma Phys. 47, 368–374.
Holst, B., Redmer, R., Desjarlais, M.P., 2008. Thermophysical properties of warm dense hydrogen using quantum molecular dynamics simulations. Phys. Rev. B 77 (18), 184201.
Holzapfel, W.B., 1969. Effect of pressure and temperature on the conductivity and ionic dissociation of water up to 100 kbar and 1000 °C. J. Chem. Phys. 50, 4424–4428.
Hubbard, W.B., MacFarlane, J.J., 1980. Structure and evolution of Uranus and Neptune. J. Geophys. Res. 85, 225–234.
Hubbard, W.B., Podolak, M., Stevenson, D.J., 1995. Interior of Neptune. In: Cruishank, D. (Ed.), Interior of Neptune, Neptune and Triton. Univ. of Arizona Press, Tucson, pp. 109–138.
Kietzmann, A., Holst, B., Redmer, R., Desjarlais, M.P., Mattsson, T.R., 2007. Quantum molecular dynamics simulations for the nonmetal-to-metal transition in fluid helium. Phys. Rev. Lett. 98, 190602.
Kohn, W., Sham, L.J., 1965. Self-consistent equations including exchange and correlation effects. Phys. Rev. 140, A1133–A1138.
Kresse, G., Furthmüller, J., 1996. Efficient iterative schemes for ab initio total-energy calculations using a plane-wave basis set. Phys. Rev. B 54, 11169–11186.
Kresse, G., Hafner, J., 1993. Ab initio molecular dynamics for liquid metals. Phys. Rev. B 47, 558–561.
Kubo, R., 1957. Statistical–mechanical theory of irreversible processes. I. General theory and simple applications to magnetic and conduction problems. J. Phys. Soc. Jpn. 12, 570–586.
Lin, J.F., Gregoryanz, E., Struzhkin, V.V., Somayazulu, M., Mao, H.K., Hemley, R.J., 2005. Melting behavior of H_2O at high pressures and temperatures. Geophys. Res. Lett. 32, L11306.
Lorenzen, W., Holst, B., Redmer, R., 2009. Demixing of hydrogen and helium at megabar pressures. Phys. Rev. Lett. 102, 115701.
Lyon, S.P., Johnson, J.D., 1992. Sesame: The Los Alamos National Laboratory Equation of State Database. Tech. Rep. LA-UR-92-3407, Los Alamos National Laboratory.
Mattsson, T.R., Desjarlais, M.P., 2006. Phase diagram and electrical conductivity of high energy-density water from density functional theory. Phys. Rev. Lett. 97, 017801.
Monkhorst, H.J., Pack, J.D., 1976. Special points for Brillouin-zone integrations. Phys. Rev. B 13, 5188–5192.
Moses, E.I., Boyd, R.N., Remington, B.A., Keane, C.J., Al-Ayat, R., 2009. The national ignition facility: Ushering in a new age for high energy density science. Phys. Plasmas 16, 041006.
Nellis, W.J., 2006. Dynamic compression of materials: metallization of fluid hydrogen at high pressures. Rep. Prog. Phys. 69, 1479–1580.
Nettelmann, N., Holst, B., Kietzmann, A., French, M., Redmer, R., Blaschke, D., 2008. Ab initio equation of state data for hydrogen, helium, and water and the internal structure of Jupiter. Astrophys. J. 683, 1217–1228.
Nettelmann, N., Kramm, U., Redmer, R., Neuhäuser, R., 2010. Interior structure models of GJ 436b. Astron. Astrophys., in press.
Oganov, A.R., Price, G.D., Scandolo, S., 2005. Ab initio theory of planetary materials. Z. Kristallogr. 220, 531–548.
Perdew, J.P., Burke, K., Ernzerhof, M., 1996. Generalized gradient approximation made simple. Phys. Rev. Lett. 77, 3865–3868.
Podolak, M., Reynolds, R.T., 1981. On the structure and composition of Uranus and Neptune. Icarus 46, 40–50.
Podolak, M., Hubbard, W.B., Stevenson, D.J., 1991. Model of Uranus' interior and magnetic field. In: Uranus. University of Arizona Press, Tucson, AZ, pp. 29–61.
Podolak, M., Podolak, J.I., Marley, M.S., 2000. Further investigations of random models of Uranus and Neptune. Planet. Space Sci. 48, 143–151.
Saumon, D., Chabrier, G., van Horn, H.M., 1995. An equation of state data for low-mass stars and giant planets. Astrophys. J. Suppl. Ser. 99, 713–741.
Schwager, B., Boehler, R., 2008. H_2O: Another ice phase and its melting curve. High Press. Res. 28, 431–433.
Schwager, B., Chudinovskikh, L., Gavriliuk, A., Boehler, R., 2004. Melting curve of H_2O to 90 GPa measured in a laser-heated diamond cell. J. Phys.: Condens. Matter. 16, S1177–S1179.
Schwegler, E., Sharma, M., Gygi, F., Galli, G., 2008. Melting of ice under pressure. Proc. Natl. Acad. Sci. 105, 14779–14783.
Stanley, S., Bloxham, J., 2004. Convective-region geometry as the cause of Uranus' and Neptune's unusual magnetic field. Nature 428, 151–153.
Stanley, S., Bloxham, J., 2006. Numerical dynamo models of Uranus' and Neptune's magnetic fields. Icarus 184, 556–572.
Stevenson, D.J., 1982. Interiors of the giant planets. Annu. Rev. Earth Planet. Sci. 10, 257–295.
Zharkov, V.N., Trubitsyn, V.P., 1978. Physics of Planetary Interiors. Parchart, Tucson.